Clays and Clay Minerals, Vol. 52, No. 4, 473–483, 2004.

MIXED-LAYER KAOLINITE-SMECTITE MINERALS IN A RED-BLACK SOIL SEQUENCE FROM BASALT IN SARDINIA (ITALY)

SIMONA VINGIANI[1], DOMINIQUE RIGHI[2,*] SABINE PETIT[2] AND FABIO TERRIBILE[1]

[1] DISSPA, Università di Napoli Federico II, Facoltà di Agraria, Via Università 100, 80055 Portici (NA), Italy
[2] UMR-CNRS 6532 "HydrASA", Faculté des Sciences, 86022 Poitiers Cedex, France

Abstract—Clay minerals from soils of a red-black soil complex developed from basaltic parent material in Sardinia are formed along a short toposequence (200 m). At the foot of the sequence, a clay-rich, black Vertisol forms, whereas at the summit, the soil is a dark reddish-brown Inceptisol. X-ray diffraction, infrared spectroscopy (FTIR), cation exchange capacity (CEC) and permanent and variable charges analyses were used, and the data show that clay minerals varied according to soil horizon and topographic position of the soil. Clay minerals in the Inceptisol are dominated by kaolinite and mixed-layer kaolinite-smectite (K-S, K:S >0.5), whereas the Vertisol contains smectites and K-S with K:S proportions <0.5. In the Vertisol, the proportion of kaolinitic layers in the K-S increases from the C horizon (K:S ~0.35–0.40) to the Ap horizon (K:S ~0.40–0.45). This soil clay-mineral distribution, in relation to topography, is similar to that reported for other (kaolinitic) red-black (smectitic) soil associations in subtropical and tropical areas. The sequence forms by downward drainage on summits and slopes, and buildup of ions in 'lows' produces smectites. Fourier transform infrared spectra indicate that two types of smectite are formed in the C horizon of the Vertisol; one is more ferric (Fe-beidellite, nontronite), the other more aluminous. Mineralogical evolution in the soil profile (from C to Ap horizon) shows a decreasing proportion of ferric smectite layers (compared to the more aluminous smectite layers). This would indicate that ferric smectite layers are preferentially transformed (or dissolved) to give kaolinite layers, with Fe precipitating as oxides and/or oxy-hydroxides or retained partly in kaolinite layers. Because the surface properties of clay minerals are related to mineralogy, the CEC (33–41 cmol kg^{-1}) in the brown Inceptisol is ~50% pH-dependent charge while in the Vertisol up to ~75% of the CEC (48–61 cmol kg^{-1}) comes from accessible permanent charges.

Key Words—Basalt (weathering), Fe-beidellite, Italy, Mixed-layer Kaolinite-smectite, Nontronite, Red-black Soil Sequence, Sardinia, Vertisol.

INTRODUCTION

Studies concerning the origin and formation of clay minerals have gained importance in soil science because clays play an important role in determining soil physical and chemical properties (Wilson, 1999). The main processes that account for the genesis of clay minerals are the simple transformation of rock-forming phyllosilicates and neoformation, where the clay minerals form through crystallization of gels or solutions (Millot, 1964). Because basalt commonly does not contain phyllosilicates as rock-forming minerals, the clay minerals in soils developed from basaltic rocks are assumed to be newly formed products derived from weathering of rock minerals.

Weathering of basic igneous rocks in tropical and subtropical areas leads to neoformation of smectite clays which may transform into kaolinite through mixed-layer kaolinite-smectite (K-S). The transformation is governed by internal soil drainage, which in turn controls soil-solution composition. Such mineralogical evolution is well demonstrated in the so-called red-black soil complexes associating black smectitic Vertisols in the poorly drained foot-slopes and red kaolinitic soils on the freely drained hill tops. Red-black soil complexes have been described in tropical (Kantor and Schwertmann, 1974; Herbillon *et al*., 1981; Yerima *et al*., 1985; Bühmann and Grubb, 1991) and Mediterranean areas (Righi *et al*., 1999).

Smectites that form in these soil sequences are generally Fe-rich with a high tetrahedral charge (Fe-beidellite, nontronite) (Wilson, 1987). The smectite-to-kaolinite transformation involves K-S interstratifications with increasing proportions of kaolinite. Chemical transformations could involve loss of Fe from the smectite structure with subsequent precipitation of low-Fe kaolinite and secondary Fe phases (Bühmann and Grubb, 1991). Righi *et al*. (1999) described the pedogenic formation of K-S in a soil toposequence developed from basaltic material in Sardinia. Mixed-layer K-S minerals showed a decreasing proportion of kaolinite from the top (70%) to the base (30%), and the smectite component was nearly identical over the soil toposequence. The smectite component was the same with respect to charge magnitude and chemical composition, independent of the proportion of smectite and kaolinite components. The aim of this study was to provide additional results to substantiate the formation of smectites and K-S in red-black soil complexes in

* E-mail address of corresponding author:
dominique.righi@hydrasa.univ-poitiers.fr
DOI: 10.1346/CCMN.2004.0520408

Copyright © 2004, The Clay Minerals Society

https://doi.org/10.1346/CCMN.2004.0520408 Published online by Cambridge University Press

Mediterranean areas. This report describes the formation of various smectites by weathering of basalts, and it details the K-S that forms from these smectites in better drained and summit positions of the land surface. The permanent charge is the greater component of the clay surface charge in smectite, but the variable charge dominates in kaolinite. Such surface-charge characteristics are probably the most important property affecting the chemical and physical behavior of soils and are ultimately related to soil fertility.

MATERIALS AND METHODS

Soil sequence

The study area lies in central Sardinia, Italy (40º12′N, 8º55′E), near the village of Sedilo (Nuoro) (Figure 1a). Geomorphology at the site is typical of a basaltic plateau, with elevations ranging from 306 to 312 m above sea level. The rock substrate is an intra-plate basalt emitted during extensional tectonics, K/Ar dated 2.95±0.10 My (Beccaluva *et al*., 1985). Mineralogical data (Porcu, 1983) indicate that it is an olivine-basalt composed of monoclinic pyroxenes and labradoritic plagioclases. The climate is Mediterranean, with a mean annual rainfall of 699 mm, (with an average seasonal rainfall of 291 mm in autumn, 217 mm in winter, 124 mm in spring, and 67 mm in summer), average annual air temperature of 13.5ºC (with seasonal temperature of 10.6ºC in autumn, 7.2ºC in winter, 15.1ºC in spring, and 21.3ºC in summer) (Ente Autonomo del Flumendosa, 1998) and average annual potential evapotranspiration of 740 mm (Thornthwaite and Mather, 1957). The area is used primarily for wheat production.

The soils are situated along a 200 m long toposequence, with a very small change in elevation (~3 m) (Figure 1b). Two soils, located at the summit and at the foot of the slope of the sequence, were described and sampled for analysis. The soils are classified (Soil Survey Staff, 1999) as a Ruptic-Lithic Haploxerept (summit and slope) and a Typic Haploxerert (slope-foot), respectively. The soil temperature and the soil moisture regimes are estimated to be thermic and xeric, respectively. The sequence is similar to a red-black complex, with the same range of colors indicated by Bühmann and Grubb (1991) for a red-black complex in South Africa. Table 1 gives a short description of the two soils, which are end-members of this toposequence. Except for minor eolian dust deposition at the soil surface, no or very limited contamination by allochtonous material is assumed, because the basaltic plateau is located in an elevated topographic position and the emission of that lava flow represents the latest volcanic event in the area.

Methods

Bulk soil samples were analyzed using MIPAF (Ministero delle Politiche Agricole e Forestali, 2000) methods: particle-size analysis was carried out by the pipette method after dispersion with Na hexametaphosphate, pH was determined in H_2O (10 g soil/25 mL water), CEC by NH_4 acetate at pH 7, exchangeable cations by atomic absorption spectrometry (AAS), and organic matter by the Walkley-Black method. Amorphous and/or crystalline Fe oxides and hydroxides were extracted with the dithionite-citrate-bicarbonate (DCB) treatment (Mehra and Jackson, 1960) and determined by AAS.

The clay (<2 μm) fraction was obtained from the soil horizons by centrifugation after removal of organic matter with dilute H_2O_2 and Na saturation by contact with 1 N NaCl solution and washing until chloride-free. The fine clay (<0.1 μm) fraction was obtained from the total clay fraction using a Beckman J2-21 centrifuge equipped with the JCF-Z continuous flow rotor.

Samples for mineralogical analysis were Ca saturated and solvated with ethylene glycol (EG) or K saturated,

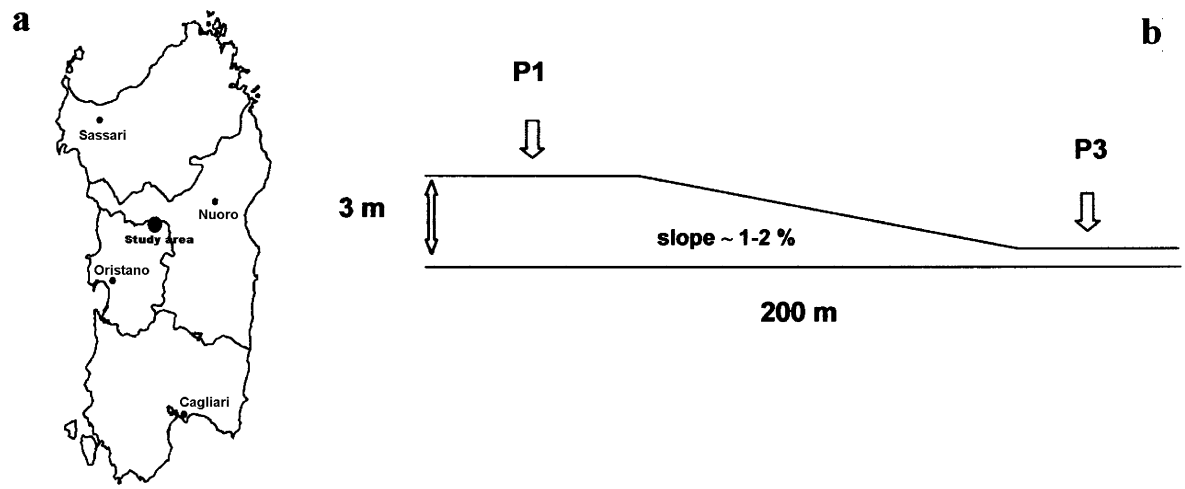


Figure 1. (a) Map of the study area; (b) schematic representation of the soil sequence with locations of the studied soils.

https://doi.org/10.1346/CCMN.2004.0520408 Published online by Cambridge University Press

Table 1. Description of the two soil profiles.

	Depth (cm)	Description and comments
Profile 1		Summit
Ap	0–22	Clay loam, dark brown (7.5 YR 3/3 moist), hard when dry, strong medium subangular blocky structure, coarse fragments ~25%, no HCl effervescence, common medium and fine roots, linear abrupt boundary.
Bw1	22–34	Clay loam, dark brown (7.5 YR 3/3 moist), hard when dry, strong medium angular blocky structure, coarse fragments ~30%, no HCl effervescence, few medium and fine roots, linear clear boundary.
Bw2	34–38	Clay, dark brown (7.5 YR 3/2), hard when dry, strong medium angular blocky structure, coarse fragments ~35%, no HCl effervescence, few fine roots, irregular abrupt boundary.
R	>38	Fissured weathered basaltic rock.
Profile 3		Foot of the slope
Ap	0–20	Clay, very dark grayish brown (10 YR 3/2), hard when dry, large cracks (2 cm wide), strong medium subangular blocky structure, coarse fragments ~2%, no HCl effervescence, abundant fine roots, linear abrupt boundary.
Bss1	20–50	Clay, very dark grayish brown (10 YR 3/2), very hard when dry, large cracks (1–2 cm wide), strong medium angular blocky structure, large peds have slickensides, coarse fragments ~1%, no HCl effervescence, common fine roots, undulate abrupt boundary.
Bss2	50–100	Clay, very dark grayish brown (10 YR 3/2), very hard when dry, large cracks (2 cm wide), sphenoidal wedge structure, large peds have slickensides, coarse fragments ~1%, no HCl effervescence, few fine roots, clear abrupt boundary.
C	100–110	Sandy clay loam, dark brown (10 YR 3/3), hard when dry, massive structure, no HCl effervescence, few fine roots, clear abrupt boundary.
R	>110	Coherent weathered basaltic rock.

heated at 350ºC and glycolated. Oriented samples were prepared by slow evaporation of the clay suspension on glass slides. X-ray diffraction (XRD) patterns were obtained using a Philips diffractometer with Fe-filtered CoKα radiation, the divergence slit being 1º and the length of sample in the diffractometer was 3 cm. A DACO-MP recorder associated with a microcomputer using the Diffrac AT software (Socabim) was used to record XRD patterns which were analyzed for their elementary component curves using a decomposition program (DecompXR, Lanson, 1993) according to the recommended procedure (Lanson, 1997). Subtraction of the background is achieved by linear interpolation between two data points defining the domain of interest (no Lorentz or polarization correction). The number of elementary curves to be fitted is increased progressively until a 'good' fit is obtained. That means that the general shape of the experimental curve is reproduced, the sum of all fitted elementary curves varies within the experimental noise, and the diffraction peak tails are modeled correctly. The profile shape of the elementary curve can be Gaussian or Lorentzian. The origin of these different curve shapes is unknown. However, better crystallized clay minerals such as mica-like phases are shown to exhibit Lorentzian-shaped curves. The XRD patterns were simulated using the NEWMOD© program (Reynolds, 1985) in order to identify and quantify accurately the mixed-layer minerals. Simulations were carried out for mixed-layer materials with various proportions of smectite and with N (number of layers in the stacking sequence) taken in the range of 5–7 (Table 2). The simulation make it possible to identify the K-S according to the similarity between experimental and simulated curves.

The layer charge of the 2:1 expandable layers was evaluated using the empirical method proposed by Olis *et al.* (1990), which makes it possible to determine the mean layer charge from d values obtained after expansion through intercalation of a single long-chain

Table 2. Positions of 001/002 reflections, d (nm), for $R0$ kaolinite/EG-smectite with N = 5–7.

% kaolinite in K-S	d (nm), N = 5–7
0	0.866
10	0.860
20	0.855
30	0.844
40	0.838
50	0.827
60	0.819
70	0.807
80	0.793
90	0.775
100	0.745

https://doi.org/10.1346/CCMN.2004.0520408 Published online by Cambridge University Press

alkylammonium ($nC = 12$) ion. To apply this method to the expandable component in K-S mixed layers, the d_{001} values were determined (using NEWMOD©, as indicated by Righi *et al*., 1999) for three-component mixed layers made of bilayer (1.77 nm) and monolayer (1.36 nm) complexes (or pseudotrilayer, 21.7 nm, and bilayer complexes) in fixed proportions, and kaolinite layers in the proportion observed in K-S in these samples (40%).

The Greene-Kelly (1953) test, which involves the suppression of the octahedral charge in dioctahedral smectite by Li saturation and heating at 300ºC, was used to distinguish tetrahedral (beidellite/nontronite) from octahedral charged smectites (montmorillonite).

The CEC of the fine clay fraction was measured using Mg^{2+} saturation of samples and removal of excess Mg salt ($MgCl_2$) with ethanol. Magnesium was replaced by NH_4^+ and analyzed by AAS in the exchange solution. The Anderson and Sposito (1991) method was used to distinguish between accessible, structural, permanent charge and variable charge. Structural charge was measured by quantifying the Cs^+ retained selectively after Cs^+-saturated clays were subjected to an exchange reaction with Li^+.

The total Fe content of the soil fraction (<2 mm) and total chemical analysis on the fine clay fractions were performed following the procedure described by Jeanroy (1972). Samples were melted at 1100ºC with Sr metaborate in an induction furnace, followed by dissolution of the glass pearl in dilute HCl. The AAS was used to analyze for Si, Al, Fe, Ti, Mg, Ca, Na and K.

Fourier transform infrared spectroscopy was performed on KBr disks prepared by mixing 1 mg of fine (<0.1 μm) clay with 300 mg of KBr and pressing at 13 kg cm^{-2}. KBr disks were heated at 110ºC overnight to remove adsorbed water and the FTIR spectra recorded using a Nicolet 510 spectrometer.

RESULTS

Soil analysis

Chemical and physicochemical analyses (Table 3) demonstrate clear differences between profile 1 (P1) and profile 3 (P3). The clay content in the P1 soil horizons (298–328 g kg^{-1} at surface, 511 g kg^{-1} at depth) is less than in the P3 horizon (607–639 g kg^{-1} in upper horizons, 246 g kg^{-1} in C). Soil pH increases from acidic (6.2–6.3) in P1 to slightly acidic (6.7 Ap) in surface horizons and sub-alkaline (7.9–8.1) in B and C horizons of P3. The CEC increases from 20.9–36.4 $cmol_{(+)}kg^{-1}$ in P1 to 44.5–46.3 $cmol_{(+)}$ kg^{-1} in most horizons in P3, and 29.6 $cmol_{(+)}$ kg^{-1} in C. The proportion of Na^+, K^+ and Ca^{2+} on the exchange sites decreases, whereas the Mg^{2+} increases, from the top to the bottom of the P1, while in the P3 the proportion of Na^+ and Ca^{2+}, together with Mg^{2+}, increases with depth.

The profiles P1 and P3 show similar total Fe content, both in rock (total Fe_2O_3 is 106 g kg^{-1} of total 105ºC dry sample in P1 and the 132 g kg^{-1} in P3) and soil (58–86 g kg^{-1} in P1, 53–96 g kg^{-1} in P3) samples. In both profiles, the total Fe content decreases from the rock to soil horizons.

The DCB-extractable Fe content is quite constant in both P1 (DCB Fe_2O_3 is 49–55 g kg^{-1} of total 105ºC dry sample) and P3 (21–26 g kg^{-1}), but higher in P1 than in P3 (Table 3). The difference calculated between total and DCB Fe content is lower in P1 (between 9 and 31 g kg^{-1}) than in P3 (between 27 and 75 g kg^{-1}), indicating that Fe in P3 is more abundant in silicates, while Fe in P1 is present mainly in oxides and oxy-hydroxides.

The XRD patterns (not shown) obtained from fine sand and silt fractions (200–2 μm) of soil horizons and rock fragments show diffraction peaks of anorthite and albite (0.447, 0.406, 0.377, 0.366, 0.320 and 0.182 nm). Soil surface horizons also show diffraction peaks of

Table 3. Characteristics of the soil horizons.

Horizon	Depth cm	Clay (<2 μm) g kg^{-1}	OM g kg^{-1}	pH H_2O	CEC cmol $_{(+)}$ kg^{-1}	Na	K	Ca	Mg	Fe_2O_3 g kg^{-1}		
						% CEC				Total	DCB	Total minus DCB
Profile 1												
Ap	0–22	298	42	6.3	20.9	5.8	1.8	51.3	27.0	58	49	9
Bw1	22–34	328	29	6.2	21.7	4.5	1.2	45.8	29.0	67	52	15
Bw2	34–38	511	23	6.3	36.4	3.8	0.9	42.4	33.3	86	55	31
R										106		
Profile 3												
Ap	0–20	607	45	6.7	45.5	7.0	1.0	49.6	38.4	53	26	27
Bss1	20–50	639	29	7.9	46.3	14.7	0.8	52.9	47.3	73	25	48
Bss2	50–100	615	18	7.9	44.6	22.5	0.6	54.1	51.8	74	–	–
C	100–110	246	08	8.1	29.6	24.0	0.5	52.6	48.3	96	21	75
R										132		

Clay and OM (organic matter): g kg^{-1} 105ºC dry soil. CEC: cmol $_{(+)}$ kg^{-1}. Na, K, Ca, Mg: exchangeable cations. Total content and DCB-extractable Fe as g kg^{-1} of 105ºC dry sample. DCB: dithionite-citrate-bicarbonate extraction.

https://doi.org/10.1346/CCMN.2004.0520408 Published online by Cambridge University Press

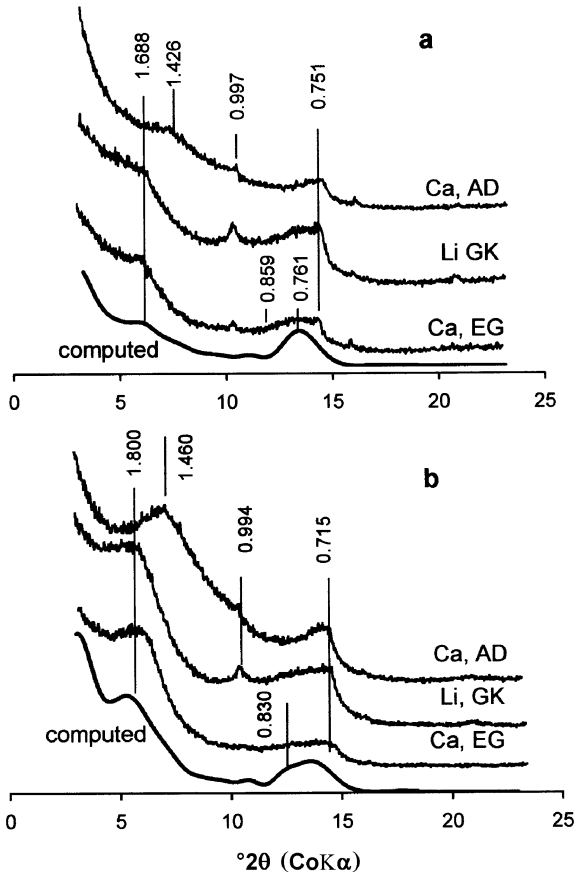


Figure 2. XRD pattern of the fine clay fraction (<0.1 μm) from profile P1. Ca, AD = Ca saturation, air-dried; EG = ethylene glycol solvated; Li, GK = Li saturation, Greene-Kelly test. (a) Ap horizon; computed: simulation for a mixture of 90% K-S (90% K, N = 5–7) and 10% K-S (30% K, N = 5–7); (b) Bw_2 horizon; computed simulation for a clay mixture including 50% kaolinite (N = 5–7) and 50% K–S (50% K, N = 5–7). d values in nm. CoKα radiation. Oriented samples.

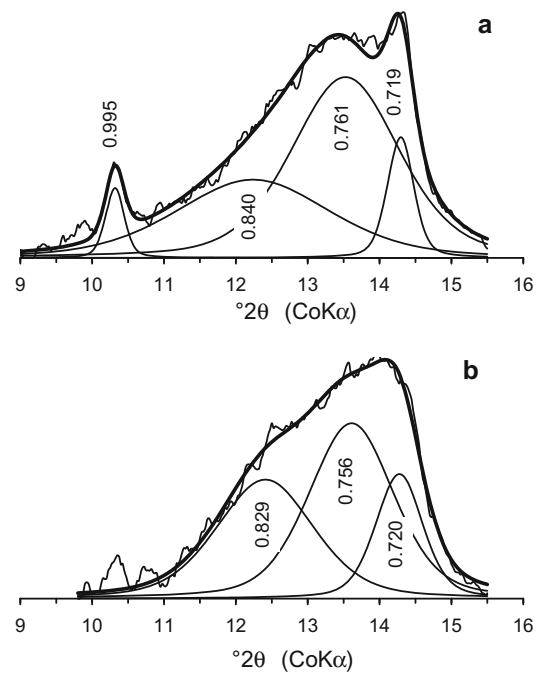


Figure 3. Decomposition of XRD pattern of the fine clay from profile P1 in the 9–16º2θ region. (a) Ap horizon; (b) Bw2 horizon. d values in nm. Ethylene glycol-solvated. Oriented samples. ——: elementary curve; ——: best fit computed curve; ~~~: experimental curve.

quartz (0.425 and 0.334 nm) thought to come from eolian allochthonous contamination. No phyllosilicates were found in sand or silt samples.

XRD of fine clay fractions

Profile P1. Figure 2a shows XRD patterns obtained from oriented specimens of the Ap horizon. The quality of the XRD patterns of these soil samples is not very good, probably due to a low degree of crystallinity of the clay minerals and/or the presence of Fe oxide and oxy-hydroxide. In the Ap horizon (<0.1 μm oriented specimens), a shift of the diffraction peak at 1.426 nm in the air-dried sample to 1.688 nm in the EG-solvated sample indicates the presence of expandable layers. From the EG-solvated samples, clear features of K-S mixed-layer minerals (diffraction bands between 0.859 and 0.715 nm) and a small amount of mica (peak at 0.997 nm) were also observed. The presence of mica is attributed to contamination of upper soil horizons by eolian allochtonous material. Decomposition of the XRD pattern from EG-solvated sample in the 9–16º2θ region (Figure 3a) gives four main elementary curves. The peak at 0.995 nm is attributed to mica, and the peak at 0.719 nm to kaolinite. The peak at 0.761 nm is attributed to K-S with 90–95% kaolinite layers, assuming N = 5–7. The peak at 0.840 nm is attributed to K-S with 30% kaolinite layers (N = 5–7). The results from the decomposition procedure suggest that the sample is a mixture of several mineral phases: mica, kaolinite and K-S with 90–95 and 30% kaolinite layers, respectively. To check the veracity of this interpretation, the XRD pattern of a mixture of two K-S was simulated using the 'Mixer' function of NEWMOD©. Simulation of K-S was carried out with N = 5–7 layers, because it produces good agreement between peak width of the simulated pattern and elementary curves from decomposition. As shown in Figure 2a, there is an acceptable match between the experimental pattern and the pattern that models a mixture of 90% K-S (90% K, N = 5–7) and 10% K-S (30% K, N = 5–7).

The XRD pattern of Bw2 horizon (Figure 2b, EG-solvated sample) is very similar to that of the Ap: the presence of expandable layers (peak at 1.800 nm), mica (peak at 0.994 nm), and features of K-S minerals

https://doi.org/10.1346/CCMN.2004.0520408 Published online by Cambridge University Press

(diffraction peaks between 0.830 and 0.715 nm). The XRD pattern decomposition in the 9−16º2θ region (Figure 3) gives three main elementary curves. The peak at 0.720 nm is attributed to kaolinite. The peak at 0.756 nm is attributed to K-S with 90−95% kaolinite layers (N = 5−7), and the peak at 0.829 nm to K-S with 50% kaolinite layers (N = 5−7). As for the Ap sample, a clay mixture including 50% kaolinite (N = 5−7) and 50% K-S (50% K, N = 5−7) was modeled with NEWMOD© (Figure 2b), which produces an acceptable match with the experimental pattern. In both the Ap and Bw2 horizons, a major component of the clay mixture is kaolinite and/or K-S with 90−95% kaolinite layers, which is associated with a K-S with a lower proportion of kaolinite layers (30% in Ap, 50% in Bw2).

Decomposition of XRD patterns from random powder samples of Ap and Bw2 horizons in the 70−75º2θ region (Figure 4a,b) shows three main elementary curves with peaks at 0.150 nm attributed to dioctahedral aluminous smectite, at 0.149 nm attributed to kaolinite and at 0.154 nm attributed to quartz.

Localization of the layer charge, either in the octahedral or tetrahedral sheet, was determined using the Li treatment. The XRD pattern of Li-treated samples of both Ap and Bw2 horizons (Figure 2a,b), compared to the untreated, are unchanged, indicating that K-S has an expandable component that is beidellitic (re-expansion after Li treatment).

The XRD patterns of K-saturated samples, heated at 350ºC, and EG-solvated samples show no re-expansion of expandable layers in the case of Ap (Figure 5a), and partial very weak re-expansion for the Bw2 (Figure 5b), indicating the presence of only high-charge smectite layers in the Ap sample, and of both high-charge and a small amount of low-charge layers in the Bw2 sample.

Profile P3. The XRD patterns from P3 soil samples have more intense peaks compared with those of P1. In the Ap EG-solvated sample (Figure 6a) the diffraction peak at 1.724 nm indicates the presence of expandable layers. The peak at 0.715 nm is attributed to kaolinite and the

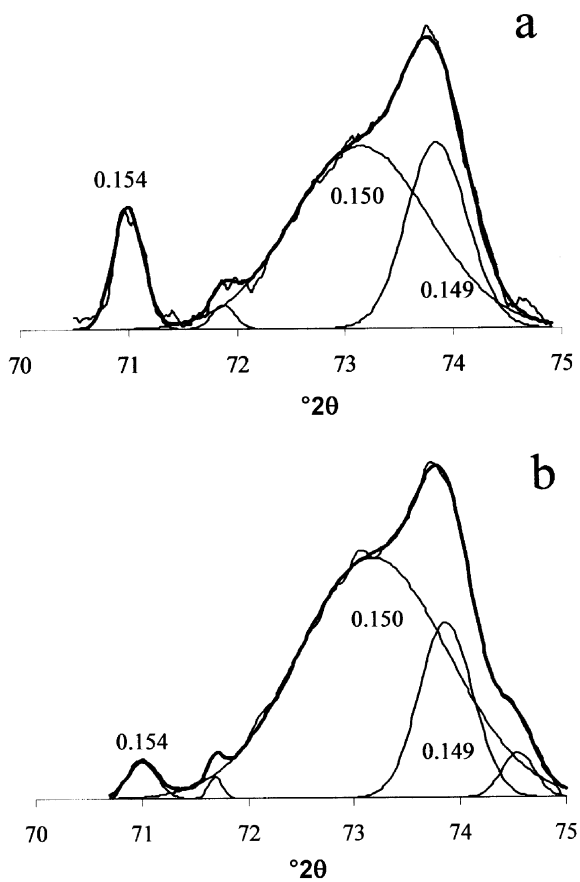


Figure 4. Decomposition of the XRD pattern of the fine clay from profile P1 in the 70−75º2θ region. (a) Ap horizon; (b) Bw2 horizon. d values in nm. Random powder. CoKα radiation.

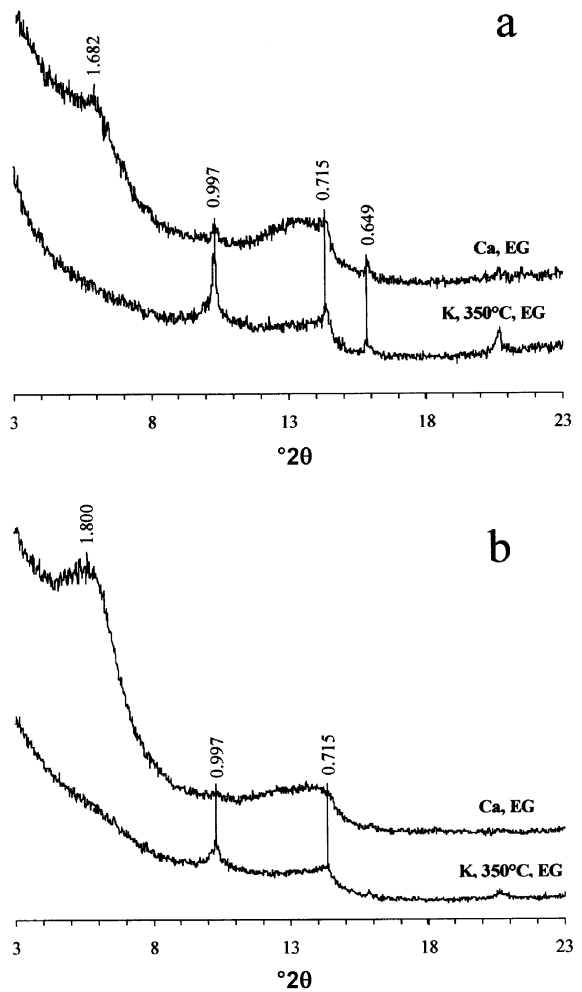


Figure 5. XRD pattern of the fine clay from profile P1 (Ca = Ca saturation; EG = ethylene glycol solvated; K, 350ºC = K saturation, heating to 350ºC). (a) Ap horizon; (b) Bw_2 horizon. d values in nm. CoKα radiation. Oriented samples.

https://doi.org/10.1346/CCMN.2004.0520408 Published online by Cambridge University Press

pattern between 0.835 and 0.715 nm indicates features of K-S. Decomposition of the XRD pattern of the EG-solvated sample in the 9–16º2θ region (Figure 7a) gives four main elementary curves. The peak at 0.995 nm is attributed to mica particles. The peak at 0.834, which shows the greatest intensity, is attributed to K-S with 40–45% kaolinite layers, assuming $N = 5–7$. The peak at 0.719 nm is attributed to kaolinite and that at 0.748 nm to K-S with 95% kaolinite layers ($N = 5–7$). The experimental XRD pattern is well modeled (using NEWMOD©) by a K-S with 40% kaolinite layers (Figure 6a).

Decomposition of the XRD powder pattern shows three main elementary curves (Figure 8a). The peak at 0.149 nm is attributed to kaolinite and that at 0.154 nm to quartz. The peaks at 0.152 and 0.151 nm are attributed to Fe- and Al/Fe-bearing dioctahedral smectites, respectively. The elementary curve with its maximum at 0.152 nm may look artificial and produced by the mathematical decomposition procedure; however, this peak position is typical for Fe-rich dioctahedral smectites which are present in the sample (especially in the C horizon) as demonstrated by the FTIR spectra (see below).

The XRD pattern of a sample subjected to the Greene-Kelly test (Figure 6a,b) shows a clear re-expansion (peak at 1.740 nm, Ap and 1.682 nm, C) indicating that the expandable component in the K-S is beidellitic (*i.e.* indicates the presence of a tetrahedral charge).

The XRD pattern of the K-treated sample indicates the presence of both high- and low-charge smectite layers (Figure 9). Because its intensity has increased following K saturation and heating (compared to that of the equivalent Ca-saturated sample), the peak at 0.994 nm is attributed to mica and vermiculite.

After intercalation of alkylammonium (nC = 12) ions, decomposition of the XRD pattern exhibits two diffraction curves with maxima at 2.23 and 1.81 nm (Figure 10a), which allows us to calculate a mean layer charge of 0.57 (2.23 nm) and 0.33 (1.81 nm) per half unit-cell, respectively, attributed to smectite layers in K-S.

The results of XRD analysis of the deep horizon (C) are very similar to those observed for the surface. The

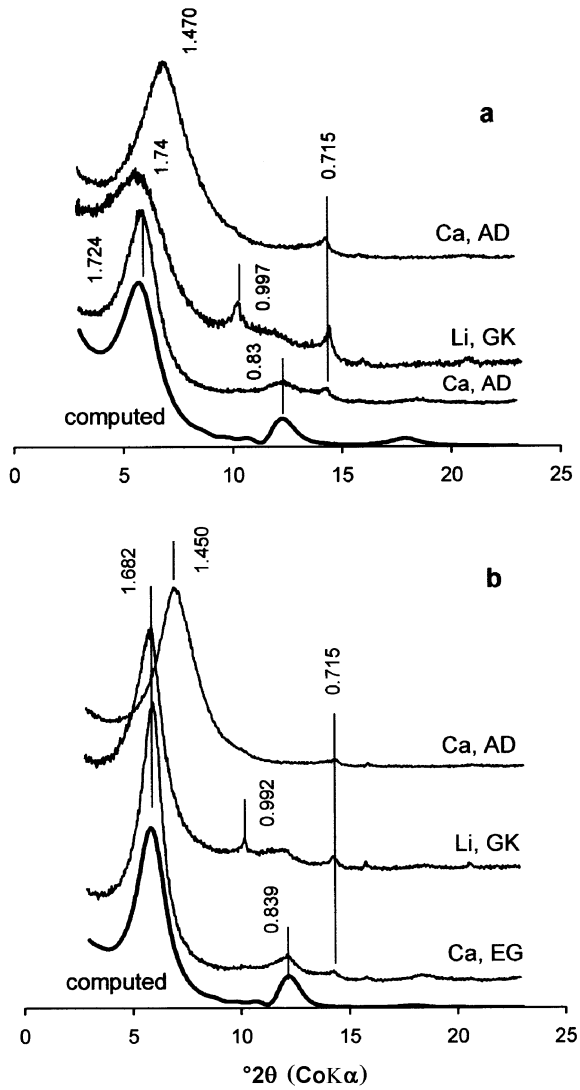


Figure 6. XRD pattern of the fine clay from profile P3. Ca = Ca saturation; EG = ethylene glycol solvated; Li, GK = Li saturation, Greene-Kelly test. (a) Ap horizon; computed: simulation of K-S with 40% kaolinite layers ($N = 5–7$); (b) C horizon; computed: simulation of K-S with 30% kaolinite layers ($N = 5–7$). d values in nm. CoKα radiation. Oriented samples.

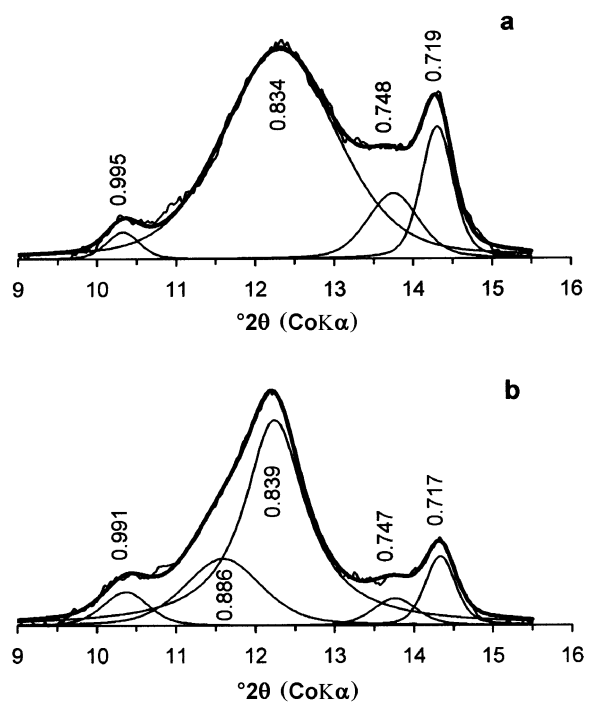


Figure 7. Decomposition of the XRD pattern of the fine clay from profile P3 in the 9–16º2θ region. (a) Ap horizon; (b) C horizon. d values in nm. CoKα radiation. Oriented samples.

https://doi.org/10.1346/CCMN.2004.0520408 Published online by Cambridge University Press

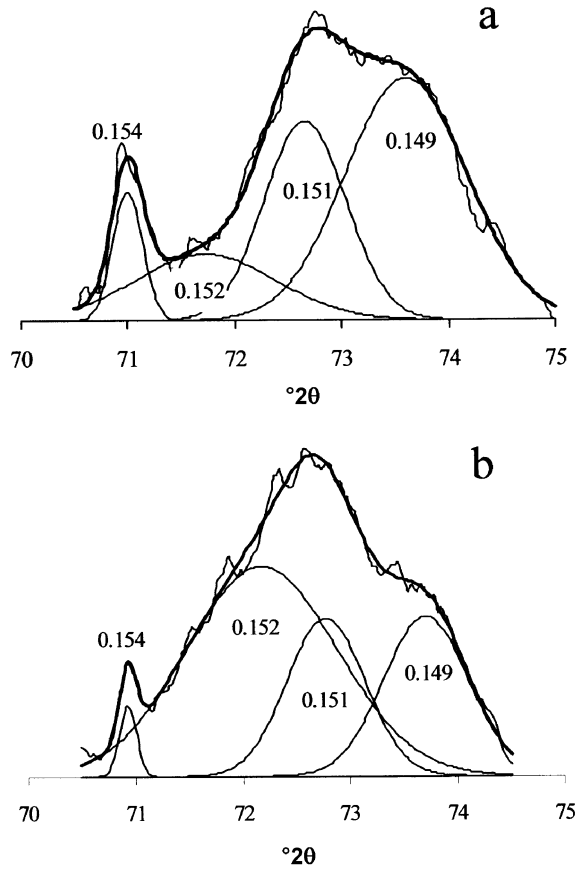


Figure 8. Decomposition of the XRD pattern of the fine clay from profile P3 in the 70–75°2θ region. (a) Ap horizon; (b) C horizon. *d* values in nm. Random powder. CoKα radiation.

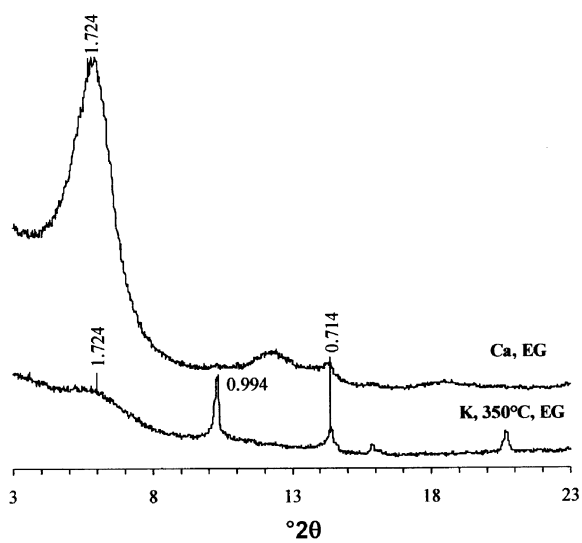


Figure 9. XRD pattern of the fine clay from profile P3, Ap horizon (Ca = Ca saturation; EG = ethylene glycol solvated; K, 350°C = K saturation, heating to 350°C). *d* values in nm. CoKα radiation. Oriented samples.

diffraction pattern of the EG-solvated sample (Figure 6b) shows the peak at 1.682 nm, attributed to expandable minerals, the peak at 0.715 nm to kaolinite, and the broad band at ~0.839 nm indicates features of K-S mixed layers. The XRD pattern decomposition (Figure 7b) gives five elementary curves. The peak at 0.991 nm is attributed to mica. The peak at 0.839 nm is attributed to K-S with 35–40% kaolinite layers (N = 5–7). The peak at 0.747 is attributed to K-S with 95% kaolinite layers, (N = 5–7) and that at 0.717 nm to kaolinite. No satisfactory interpretation was found for the peak at 0.886 nm, which looks artificial and produced by the mathematical decomposition procedure. Using NEWMOD©, a good simulation of the experimental pattern was obtained for K-S with 30% kaolinite layers (N = 5–7). In both the Ap and C horizons, the proportion of kaolinite in the K-S is <50%, and slightly higher in the Ap than in the C sample.

The XRD powder patterns confirm the presence of Fe- and Al/Fe-bearing dioctahedral smectites (peaks at 0.152, 0.151 nm), but the intensity of the peak attributed to the Fe-rich component is greater than for Ap horizon, indicating a larger amount of Fe-smectites. The results of the diffraction analysis carried out on K-saturated and heated samples (not shown) indicates the presence of both high- and low-charge smectite layers (partial re-expansion) and the XRD pattern for Li-treated samples (Figure 6b) indicates that the expandable component in the K-S is beidellitic.

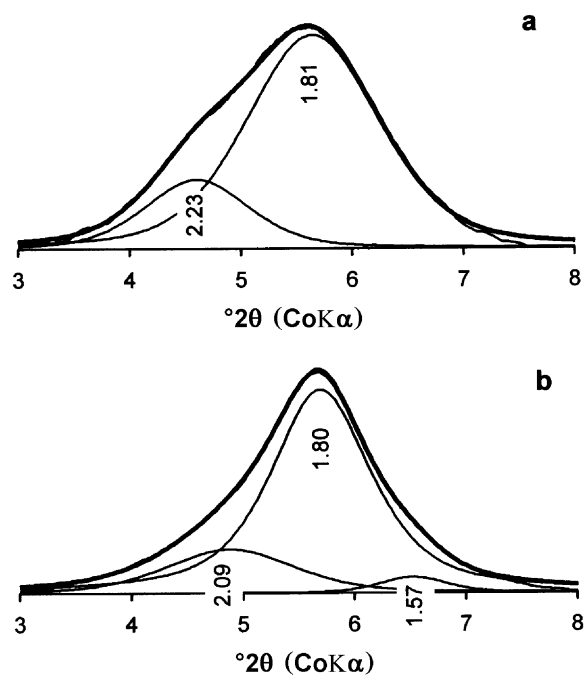


Figure 10. Decomposition of the XRD pattern of the fine clay saturated with alkylammonium ion (nC = 12) from profile P3 in the 3–8°2θ. region. (a) Ap horizon; (b) C horizon. *d* values in nm. CoKα radiation. Oriented samples.

https://doi.org/10.1346/CCMN.2004.0520408 Published online by Cambridge University Press

Decomposition of the XRD pattern of the alkyl-ammonium-treated sample gives three curves with maxima at 2.09, 1.80 and 1.57 nm, which gives a mean layer charge of 0.52 (2.09 nm), 0.33 (1.80 nm) and 0.28 (1.57 nm) per half unit-cell, respectively, attributed to smectite layers.

Cation exchange capacity

The CEC of the fine clay fraction increases from the surface to the deepest horizons for both P1 (34 $cmol_{(+)}kg^{-1}$, Ap; 41 $cmol_{(+)}kg^{-1}$ Bw2) and P3 (48 $cmol_{(+)}kg^{-1}$ Ap; 61 $cmol_{(+)}kg^{-1}$ C), and the CEC of soil horizons from P3 is greater than that measured for the P1 samples (Table 4). In both P1 and P3, the contribution of variable charge to the total CEC is very similar and accounts for 15.8–18.5 $cmol_{(+)}kg^{-1}$. The accessible permanent charge is higher in P3 (32.5– 41.8 $cmol_{(+)}kg^{-1}$) than in P1 (7.2–23.8 $cmol_{(+)}kg^{-1}$), representing 65–70% and 50–56% of the total charge, respectively.

FTIR spectroscopy

For the P1 profile, in both the Ap and Bw2 horizons, the spectra clearly show the sharp νAl_2OH doublet, characteristic of kaolinite, at 3700 and 3622 cm^{-1} (Figure 11). The kaolinite features are superimposed on other bands: a very broad band centered near 3420 cm^{-1} due to water and a broad band centered near 3600 cm^{-1} due to smectite. The position of that band, which is probably multicomponent, shows that the smectite is aluminous and contains Fe (Madejová *et al.*,

Table 4. CEC values of the fine clay fraction.

Horizon	CEC	VC	APC
		$cmol_{(+)}\ kg^{-1}$	
Profile 1			
Ap	34	17.3	17.2
Bw1	33	15.8	17.3
Bw2	41	18.5	23.8
Profile 3			
Ap	48	17.3	32.5
Bss1	57	17.7	40.4
Bss2	56	18.1	36.7
C	61	16.0	41.8

VC: variable charge
APC: accessible permanent charge

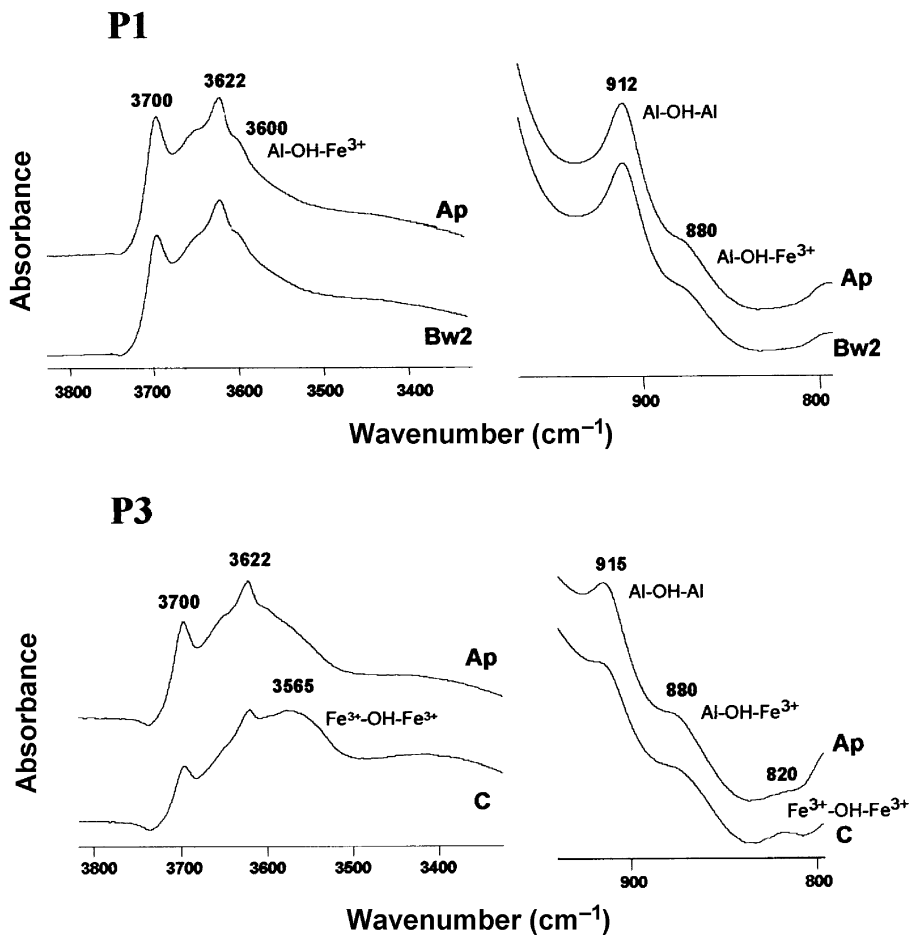


Figure 11. FTIR spectra of the fine clay from profiles P1 and P3.

https://doi.org/10.1346/CCMN.2004.0520408 Published online by Cambridge University Press

1994). This in accordance with the δOH region where a δAl_2OH band due to both kaolinite and smectite, and a δAlFeOH band due to smectite are observed. For the Ap horizon of the P3 profile (Figure 11) the spectrum exhibits kaolinite features. However, compared to the P1 profile, the smectite component is relatively enhanced. Moreover, the position of the broad band due to smectite shifts toward the lower wavenumber side, meaning that the smectite is enriched in Fe (Madejová *et al*., 1994). For the C horizon (Figure 11) the kaolinite component is less intense than for the Ap horizon whereas the smectite features are relatively more pronounced. Moreover, the broad band due to smectite clearly shifts toward lower wavenumbers meaning that the smectite is richer in Fe. The maximum of the broad multicomponent band at 3565 cm^{-1} is mainly due to the occurrence of a $\nu Fe_2^{3+}OH$ component in accordance with the δOH region where a $\delta Fe_2^{3+}OH$ band is observed at 820 cm^{-1}. Based on FTIR data, the kaolinite/smectite ratio in the sample is similar in the Ap and Bw2 horizons of the P1 profile. This ratio is lower in the Ap and C horizons of the P3 profile, the lowest ratio being observed for the C horizon. In the same way the Al/Fe ratio in smectite is similar and relatively high in both the Ap and Bw2 horizons of profile P1; it is lower in the profile P3. In this profile the ratio decreases from the top (Ap horizon) to the bottom (C horizon). These results are in accordance with the XRD data.

DISCUSSION

The Sedilo soil sequence was developed from the same basaltic parent material. The presence of quartz in the fine sand and silt fractions of the upper horizons, and of trace amounts of mica and vermiculite in the fine clay, indicate a limited contamination of soils by allochtonous material due to eolian transport. Thus, as the parent material does not contain phyllosilicates, it is assumed that clay minerals in the soils are newly formed products from rock weathering.

Results from XRD analysis show the presence of K-S as the dominant clay mineral in the fine clay fractions of profile P1, and smectite and K-S with high proportion of smectite layers in the P3 profile, at the foot of the slope. The higher values of permanent structural charge observed in the P3 profile are in good agreement with clay mineralogy as characterized by XRD analysis. It confirms a greater proportion of smectites in the P3, as compared to the P1 profile where kaolinite layers are more abundant.

The DCB-extractable and total Fe contents indicate that in P3 horizons, particularly in the deepest C horizon, Fe occurs mostly in silicates, whereas in P1 horizons, Fe is present predominantly as oxide and oxyhydroxide forms. This is confirmed by the FTIR spectra showing ferric smectite layers in the fine clays from the C horizon of the P3 profile. Fe-bearing smectites, like Fe-beidellites and nontronite, are common products of basic rocks or basalt weathering (Ildefonse, 1987; Wilson, 1987) and usually confined to the lower portions of soil profiles.

The mineralogical evolution of the two end-members of the soil sequence is thought to be governed mainly by topography and resulting drainage conditions induced by the slope gradient as previously described by Righi *et al*. (1999). The K-S in soils is thought to form at the expense of smectite precursors through desilicification and increased proton activity in the soil solutions (Delvaux and Herbillon, 1995). The reaction is reported to proceed via expulsion of interlayer and layer cations, the most important being Fe (Bühmann and Grubb, 1991). In the present study, two types of smectite are formed in the C horizon of profile P3, one is more ferric, the other more aluminous. Mineralogical evolution in the soil profile (from the C to the Ap horizon) shows an increasing proportion of kaolinitic layers in the K-S and a decreasing proportion of ferric smectite layers (compared to the more aluminous smectite layers). This would indicate that ferric smectite layers are more susceptible to the desilicification process and are preferentially transformed (or dissolved) to give kaolinite layers, with Fe precipitating as oxides and/or oxyhydroxides. In the P1 profile, smectite layers are not as rich in Fe as in the P3 samples, suggesting that ferric smectites do not form or are weathered very early in this profile which is characterized by a faster internal drainage.

CONCLUSIONS

The mineralogical evolution observed in the Sedilo soil sequence is not exceptional in the Sardinian environment. The formation of mixed-layer K-S minerals with different proportions of kaolinite, and their relationship with topography and drainage conditions have been observed in another soil sequence in Sardinia. These sequences are very similar to red-black soil sequences found on basalts in tropical and subtropical areas. This suggests that the formation of red-black soil sequences with their typical K-S mineralogy is not restricted to tropical and subtropical areas but may extend to the Mediterranean climatic areas if appropriate parent materials and landscapes are present.

ACKNOWLEDGMENTS

The authors would like to thank A. Vacca, A. Aru, S. Loddo and P. Baldaccini for their essential support in choosing and sampling the study site.

REFERENCES

Anderson, S.J. and Sposito, G. (1991) Cesium-adsorption method for measuring accessible structural surface charge. *Soil Science Society of America Journal*, **55**, 1569–1576.

Beccaluva, L., Civetta, L., Macciotta, G. and Ricci, C.A.

https://doi.org/10.1346/CCMN.2004.0520408 Published online by Cambridge University Press

(1985) Geochronology in Sardinia: results and problems. *Rendiconto Società Italiana di Mineralogia e Petrografia*, **40**, 57–72.

Bühmann, C. and Grubb, P.L.C. (1991) A kaolin-smectite interstratification sequence from a red and black complex. *Clay Minerals*, **26**, 343–358.

Diaz, M.C. and Torrent, J. (1989) Mineralogy of iron oxides in two soil chronosequences of central Spain. *Catena*, **16**, 291–299.

Delvaux, B. and Herbillon, A.J. (1995) Pathways of mixed-layer kaolin-smectite formation in soils. Pp. 457–461 in: *Clays Controlling the Environment* (G.J. Churchman, R.W. Fitzpatrick and R.A. Eggleton, editors). CSIRO Publishing, Melbourne, Australia.

Ente Autonomo del Flumendosa (1998) *Nuovo studio dell'idrologia superficiale della Sardegna. Regione Autonoma della Sardegna, Assessorato della Programmazione*, (X. Bilancio, editor). Assetto del Territorio-Centro Regionale di Programmazione, Cagliari, CD-rom.

Herbillon, A.J., Frankart, R. and Vielvoye, L. (1981) An occurrence of interstratified kaolinite-smectite minerals in a red-black soil toposequence. *Clay Minerals*, **16**, 195–201.

Ildefonse, P. (1987) Analyse pétrographique des altérations prémétéoriques et météoriques de deux roches basaltiques (basaltes de Belbex, Cantal et Hawaiite de M'Bouda, Cameroun). Doctoral thesis, Université Paris 7, Paris, 142 pp.

Jeanroy, E. (1972) Analyse totale des silicates naturels par spectrométrie d'absorption atomique. Application au sol et à ses constituants. *Chimie Analytique*, **54**, 159–166.

Kantor, W. and Schwertmann, U. (1974) Mineralogy and genesis of clays in red-black toposequences in Kenya. *Journal of Soil Science*, **25**, 67–78.

Lanson, B. (1993) *DECOMPXR, X-ray Decomposition Program*. ERM, Poitiers, France.

Lanson, B. (1997) Decomposition of experimental X-ray diffraction patterns (profile fitting): a convenient way to study clay minerals. *Clays and Clay Minerals*, **45**, 132–146.

Madejová, J., Komadel, P. and Čičel, B. (1994) Infrared study of octahedral site populations in smectites. *Clay Minerals*, **29**, 319–326.

Mehra, O.P. and Jackson, M.L. (1960) Iron oxide removal from soils and clays by a dithionite-citrate system buffered with sodium bicarbonate. *Clays and Clay Minerals*, **7**, 317–327.

Millot, G. (1964) *Geologie des Argiles*. Masson, Paris.

MIPAF (Ministero delle Politiche Agricole e Forestali) (2000) *Metodi di Analisi Chimica del Suolo. Collana di metodi analitici per l'agricoltura.* Franco Angeli, Italy.

Olis A.C., Malla P.B. and Douglas L.A. (1990) The rapid estimation of layer charges of 2:1 expanding clays from a single alkylammonium ion expansion. *Clay Minerals*, **25**, 39–50.

Porcu, A. (1983) Geologia del Graben di Ottana (Sardegna centrale). *Rendiconto Seminari Facoltà di Scienze dell'Università di Cagliari*, **53**, 1–32.

Reynolds, R.C. (1985) *NEWMOD: A Computer Program for the Calculation of One-dimensional Diffraction Powders of Mixed-layer Clays*. R.C. Reynolds, 8 Brook Rd., Hanover, New Hampshire 03755 USA, 315 pp.

Righi, D., Terribile, F. and Petit, S. (1999) Pedogenic formation of kaolinite-smectite mixed layers in a soil toposequence developed from basaltic parent material in Sardinia (Italy). *Clays and Clay Minerals*, **47**, 505–514.

Soil Survey Staff (1999) *Soil Taxonomy. A Basic System of Soil Classification for Making and Interpreting Soil Surveys*, 2nd edition. USDA-NRCS, Agriculture Handbook N. 436, US Government Print Office, Washington, DC.

Thornthwaite, C.W. and Mather, J.R. (1957) Instruction and Tables for Computing Potential Evapotranspiration and the Water Balance. *Publications in Climatology*, **10**, Centerton, New Jersey.

Wilson, M.J. (1987) Soil smectites and related interstratified minerals: recent developments. *Proceedings of the International Clay Conference, Denver*, pp. 167–173.

Wilson, M.J. (1999) The origin and formation of clay minerals in soils: past, present and future perspectives. *Clay Minerals*, **34**, 7–25.

Yerima, B.P.K., Calhoun, F.G., Senkayi, A.L. and Dixon, J.B. (1985) Occurrence of interstratified kaolinite-smectite in El Salvador Vertisols. *Soil Science Society of America Journal*, **49**, 462–466.

(*Received 16 October 2003; revised 18 March 2004; Ms. 846; A.E. Ray E. Ferrell, Jr.*)

https://doi.org/10.1346/CCMN.2004.0520408 Published online by Cambridge University Press